# Shell-side boiling of a glycerol-water mixture at low sub-atmospheric pressures

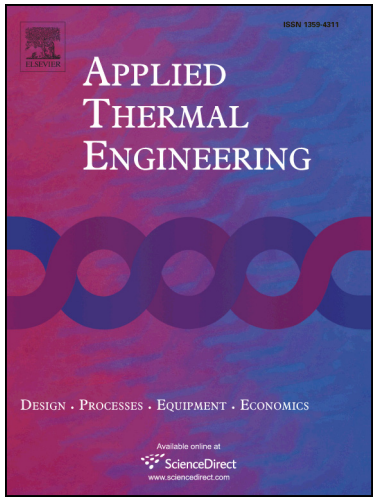


Research Paper

# Shell-side boiling of a glycerol-water mixture at low sub-atmospheric pressures

D.A. McNeil, B.M. Burnside, E.A. Elsaye, S.M. Salem, S. Baker

PII: S1359-4311(16)33587-6
DOI: http://dx.doi.org/10.1016/j.applthermaleng.2016.11.169
Reference: ATE 9580

To appear in: *Applied Thermal Engineering*

Received Date: 29 February 2016
Revised Date: 22 November 2016
Accepted Date: 23 November 2016

Please cite this article as: D.A. McNeil, B.M. Burnside, E.A. Elsaye, S.M. Salem, S. Baker, Shell-side boiling of a glycerol-water mixture at low sub-atmospheric pressures, *Applied Thermal Engineering* (2016), doi: http://dx.doi.org/10.1016/j.applthermaleng.2016.11.169

# Shell-side boiling of a glycerol-water mixture at low sub-atmospheric pressures

**D A McNeil[1*], B M Burnside[1], E A Elsaye[1], S M Salem[1] and S Baker[2]**

[1] School of Engineering and Physical Science, Heriot-Watt University

Riccarton, Edinburgh EH14 4AS, UK

[2] National Nuclear Laboratory, 5th Floor, Chadwick House, Risley, Warrington, WA3 6AE, UK

* E-mail: D.A.McNeil@hw.ac.uk

Keywords: Boiling, binary mixtures, two-phase flow, shell-side, low pressure

**Abstract**

Experimental data are reported for boiling water and a glycerol-water mixture at a free surface pressure of 50 mbar absolute on the shell-side of a thin slice model of an industrial boiler. The boiler test section was 1 m high, 0.75 m wide, 98 mm long and contained 36 electrically heated, horizontal tubes that were 28.5 mm in diameter. The design of the boiler ensured that the tubes were submerged in a liquid pool. The height of the liquid pool was set to 2 m, submerging the top of the tube bundle in 1.6 m of liquid. The heat flux was varied within the range 10-65 kW/m$^2$. A near-symmetrical half of the tube bundle contained wall thermocouples. An additional 29 thermocouples were located throughout the liquid pool.

For both fluids, the liquid temperature in the pool was found to be reasonably uniform and controlled by the pressure at the free surface. This led to subcoolings of up to 31 K on the tube surfaces. The reasonably uniform pool temperature suggests that the liquid re-circulates within it.

For water, boiling was initiated in the heat flux range 25-40 kW/m$^2$, whereas the glycerol-water mixture initiated boiled within the range 10-25 kW/m$^2$. Below these heat flux ranges, both fluids were in natural convection, with the measured wall superheats in reasonable agreement with predictions from a correlation available in the open literature. The difference in the fluids' boiling onset resulted from the natural convection, heat-transfer coefficients of the glycerol-water mixture being lower than that for water. The boiling wall superheats for water were reasonably well predicted by a correlation available in the open literature.

Boiling glycerol-water mixture data, taken at atmospheric pressure and available in the open literature, was used to identify methods for correcting pure fluid boiling heat-transfer coefficients for mixture effects. Mixture boiling superheats were reasonably well predicted by some of these methods. The method that worked best at

atmospheric pressure did not work best at low pressure. A method is identified that is reasonable at atmospheric and low pressures.

## 1. Introduction

Some evaporators, like those used to process nuclear waste, boil fluids that are highly corrosive. The corrosion rate of the materials used to construct these evaporators depends on their temperature. Thus, the life of the evaporator can be extended if the wall temperatures of the evaporator are kept low. One way of achieving this is to boil the fluid at a low pressure, and hence a low saturation temperature. The batch operation of these evaporators removes vapour, causing the remaining liquid to become more concentrated in its dissolved components. This leads to variations in the fluid's properties. This study was initiated to investigate the changes that occur in evaporator operation as the properties, particularly the viscosity, of the boiling fluid are altered. The investigation was carried out on a one-quarter scale, thin slice model of a bespoke industrial evaporator that is used in the processing of nuclear waste. The model evaporator had a glass front to allow visual information to be obtained and was operated at an absolute pressure of 50 mbar. The tests were carried out at a pool height of approximately 2 m.

McNeil et al [1] reported on tests that used water at various pressures as the test fluid in the same evaporator used in this study. They noted that the evaporator has some physical similarities to a kettle reboiler and showed that its thermo-fluid behaviour was completely different. They found that the evaporator's behaviour depended on the liquid level. At a low liquid level, fluid recirculation produced heat transfer behaviour that was compatible with subcooled flow boiling, whereas at a high liquid level, the tubes behaved in isolation to each other. For the latter case, the single-phase, heat-transfer behaviour was described by the Churchill and Chu [2] correlation and the nucleate boiling behaviour by the Gorenflo correlation [3].

Historically, pool boiling at low, vacuum level, pressures has not had very much attention in the literature. Some data have been reported. A reasonable summary of work done prior to 2008 is given by Feldmann and Luke [4]. The reduced pressure is the ratio of the pressure to the critical pressure. A value of 0.00023 was used in their study. They noted that only two data sets were reported to go that low in the literature, one by Minchenko [5] and another by Gorodov et al [6]. The Minchenko [5] heat-transfer coefficient data were shown to be more than twice the magnitude of those reported by Gorodov et al [6], with the later reasonably predicted by the Gorenflo [3] correlation and the former by the Cooper [7] correlation, with the correlation's coefficient increased in line

with the recommendation for a copper horizontal cylinder. Raben et al [8] measured boiling water, heat-transfer coefficients within the pressure range 0.013-1.013 bar and within the heat flux range 3–190 kW/m$^2$. They also viewed the boiling process with the aid of high speed photography and used a heat-transfer partition model to explain their results. The model required inputs for nucleation site density and bubble frequency that were not generalised. They observed that reducing the pressure reduced the heat-transfer coefficient.

More recently, water has been proposed at a refrigerant. This has led to boiling at low pressure becoming more topical. Typical of these studies are [9-12]. In these studies the emphasis tends to be the effect of the low pressure of the boiling surface and the bubble dynamics, with little information given on the actual heat-transfer coefficient. They report observations similar to McNeil et al [1] in that the pool height has a significant effect on the saturation pressure, and thus the saturation temperature, and that the bubbles on the boiling surface are very large because of the very low pressure of the steam produced. Yu et al [11] did present some analysis of their heat transfer coefficients obtained within the pressure range 1.8-3.3 kPa. Their correlation contained natural convection parameters. The data was obtained at relatively low heat fluxes, less than 10 kW/m$^2$, and therefore may not have involved fully-developed boiling. Zajaczkowski et al [12] measured heat-transfer coefficients for boiling water within the heat-flux range of 10-45 kW/m$^2$ and within the pressure range 1-10 kPa. Their boiling line did not deviate from the single-phase curve. This is in contrast to other studies, e.g Raben et al [8], where a significant deviation was observed. Several studies, including McNeil et al [1], have noted that boiling can be significantly delayed at low pressures. It is not clear that boiling heat transfer occurred in these tests, although the author's reported observing some bubbles breaking off the heated surface. Correlations for low pressure boiling therefore require further investigation.

The low level recirculation-type behaviour observed previously in this evaporator, [1], could be impeded by an increased liquid viscosity. Tests to investigate this are necessary and can be implemented by adding glycerol to water. However, this will have a number of important ramifications for the data, it will change other physical properties of the fluid and it will change the boiling process from one involving a pure fluid to one involving a binary mixture. While analysis of the former only requires a change in the physical property data, the latter fundamentally alters the heat-transfer mechanism. Increased viscosity is unlikely to alter the high-level, isolated-tube type behaviour previously reported for the evaporator, [1]. Therefore a high level study is likely to reveal information on the effect of the binary mixture on the boiling heat transfer process and is therefore a necessary precursor to a low level study.

The boiling of binary mixtures differs from the boiling of pure components for two main reasons, the presence of a second component substantially changes the thermodynamic and transport properties of the fluid and the presence of a more volatile component creates a concentration gradient between the bulk liquid and the liquid-vapour interface that introduces a mass-transfer diffusion process that can have significant effects on the heat-transfer process. A reasonable review of previous studies is given in [13]. What the literature reveals is that a general method for the prediction of boiling heat transfer in a binary mixture is not available. The methods so far produced depend on correlations that are frequently derived from the fluids used in their formulation and do not, in general, extend to other fluid pairs. The literature detailed herein therefore concentrates on data and methods that may have some application to water-glycerol mixtures.

Sternling and Tichacek, [14] produced some experimental data on boiling water-glycerol mixtures. They boiled several mixtures at atmospheric pressure within the heat flux range 50-450 kW/m$^2$. The pool boiling heat-transfer coefficients were measured on a stainless steel tube 4.6 mm in diameter and 89 mm long. Little analyses of the data were carried out and little in the way of recommendations were made. There appears to be few, if any, experimental data available for boiling binary mixtures at low, vacuum level pressures.

There are several design methods available that account for the presence of the second fluid. All of them try, to some extent, to build on the large body of data obtained for boiling pure components. There are, however, several different approaches.

One of the earliest approaches taken was to treat the heat-transfer coefficient, or the wall superheat, as if they were molecular properties of the liquid. This allowed existing methods to be used to determine the coefficients or superheats for the pure fluids and for an interpolation to be carried out to obtain an 'ideal' value for the mixture. A correction factor was then applied to this 'ideal' value to account for the changes in heat transfer resulting from alterations to the thermodynamic and transport properties and of any mass diffusion. The interpolation could be based on the mass or mole fraction of the more volatile component. These methods are therefore purely empirical.

Stephan and Kroner [15] proposed such a method. They suggested that the ideal wall superheat, $\Delta T_{supI}$, for the mixture could be obtained from

$$\triangle T_{supI} = X_w \triangle T_{supw} + (1 - X_w) \triangle T_{supg} \quad (1)$$

where $X_w$ was the liquid mole fraction of the most volatile component and $\Delta T_{supw}$ and $\Delta T_{supg}$ were the wall superheats obtained at the applied heat flux for the most and least volatile components respectively. A correction factor, $C_f$, was used to account for the increase in wall superheat brought about by the changes in the thermodynamic and transport properties and of any mass diffusion through,

$$C_f = 1 + C_p\left(0.88 + 1.2\frac{p}{1\times10^6}\right)|Y_w - X_w| \quad (2)$$

where $Y_w$ was the vapour mole fraction of the most volatile component and $p$ was the pressure, in pascals. The inclusion of the pressure term in Equation (2) recognised the empirical observation that the correction factor was pressure dependent. The coefficient, $C_{p,}$ was a factor introduced to make the correlation fluid specific. A value of 1.5 was suggested for glycerol-water mixtures. Making the correlation fluid specific is an indication of how difficult it is to capture the complex interactions that occur.

Unal, [16], took a similar approach. However, a more universal approach was used, correlating the data from several fluid combinations to obtain the correction factor through,

$$C_f = [1 + (B_2 + B_3)(1 + B_4)](1 + B_5) \quad (3)$$

where

$$B_2 = (1 - X_w)ln\left(\frac{1.01-X_w}{1.01-Y_w}\right) + X_w ln\left(\frac{X_w}{Y_w}\right) + |Y_w - X_w|^{1.5} \quad (4)$$

$$B_3 = 0\ for\ X_w \geq 0.01 \quad (5a)$$

$$B_3 = \left(\frac{Y_w}{X_w}\right)^{0.1} - 1\ for\ X_w < 0.01 \quad (5b)$$

$$B_4 = 152\left(\frac{p}{p_c}\right)^{3.9} \quad (6)$$

$$B_5 = 0.92|Y_w - X_w|^{0.001}\left(\frac{p}{p_c}\right)^{0.66} \quad (7)$$

in which $\frac{X_w}{Y_w} = 1\ for\ X_w = Y_w = 0$ and $p_c$ is the critical pressure. The value of the most volatile component was used. The increased complexity in this correlation is required to capture the effects induced by changes in the thermodynamic and transport properties and of any mass diffusion effects in a generalised way.

Several methods have been proposed that have some theoretical basis. Binary mixtures have two components, one of which is usually more volatile than the other. As the more volatile component vaporises, a concentration gradient develops to drive the more volatile component from the bulk fluid to the vapour-liquid interface. Most theories that have been developed involve a description of this mass transfer process. These frequently link the evaporation rate of the most volatile component to the conduction of heat from the wall to the vapour-liquid

interface. The concentration of the most volatile component is reduced at this interface, increasing the saturation temperature. Thus, the wall temperature is increases by the mass-transfer process.

A boundary layer approach to the mass transfer process has been proposed by several authors and is typified by the method proposed by Thome and Shakir, [17]. The approach envisages a boundary layer through which heat and mass transfer processes occur. They treat the effects of the changes in thermodynamic and transport properties by using mixture properties in a pure fluid correlation to give their 'ideal' heat-transfer coefficient, $\alpha_I$. The 'ideal' wall superheat followed from

$$\triangle T_{supI} = \frac{q}{\alpha_I} \tag{8}$$

where $q$ was the heat flux. The mass diffusion effects are accounted for by the introduction of a correction factor i.e.,

$$C_f = 1 + \frac{\triangle T_{bp}}{\triangle T_I}\left[1 - exp\left(-\frac{q}{\beta \rho_L h_{fg}}\right)\right] \tag{9}$$

where $\Delta T_{bp}$ was the boiling range and $\beta$ = 0.0003 m/s and is the 'typical' mass transfer coefficient for the more volatile component through the boundary layer. The heat-transfer coefficient, $\alpha$, followed from

$$\alpha = \frac{\alpha_I}{C_f} \tag{10}$$

Several attempts have been made to link changes to the boiling process directly to the mass diffusion of the most volatile component from the bulk liquid to the bubble-liquid interface. Kandlikar [18] is typical of this approach. The effects of thermodynamic and transport properties was accounted for by introducing an 'idea' heat transfer coefficient, $\alpha_{IA}$, that was evaluated from

$$\alpha_{IA} = 0.5\left(x_w \alpha_w + (1 - x_w)\alpha_g + \alpha_{cf}\right) \tag{11}$$

where $x_w$ was the mass fraction of the least volatile component and $\alpha_w$ and $\alpha_g$ were the heat-transfer coefficients of the least and most volatile components evaluated at the applied heat flux and obtained from pure fluid correlations. The correction-factor, heat-transfer coefficient, $\alpha_{cf}$, was found from

$$\alpha_{cf} = \frac{x_w}{\alpha_w} + \frac{(1 - x_w)}{\alpha_g} \tag{12}$$

This approximate 'ideal' heat-transfer coefficient is corrected to the 'ideal' value through fluid property effects thus

$$\alpha_I = \alpha_{IA}\left(\frac{T_{sata}}{T_{sat}}\right)^{0.674}\left(\frac{h_{fga}}{h_{fg}}\right)^{0.371}\left(\frac{\rho_g}{\rho_{ga}}\right)^{0.297}\left(\frac{\sigma_a}{\sigma}\right)^{0.317}\left(\frac{k_L}{k_{La}}\right)^{0.284} \tag{13}$$

where $T_{sat}$ was the saturation temperature of the bulk liquid and $h_{fg}$, $\rho_g$, σ, $k_L$ were the enthalpy of evaporation, the density of the gas, the surface tension and the liquid thermal conductivity of the mixture respectively. The corresponding approximate properties with the added subscript 'a' are the mixture properties evaluated from

$$\phi = x_w \phi_w + (1 - x_w)\phi_g \tag{14}$$

where $\phi$ is the pure fluid property. The property groups in Equation (13) were produced from the generalised pure fluid correlation of Stephan and Abdelsalam, [19]. The mass diffusion effect was accounted for by introducing a correction factor, $C_f$. This factor was determined as the ratio of vaporisation rates with and without mass diffusion and allowed the wall superheat to be determined from

$$\triangle T_{sup} = \frac{q}{C_f \alpha_I} \tag{15}$$

where

$$C_f = 1 - 64V_p \; for \; V_p \leq 0.005 \tag{16a}$$

$$C_f = \frac{0.678}{(1+V_p)} \; for \; V_p > 0.005 \tag{16b}$$

Bubble growth is a transient process for both heat and mass transfer. The parameter $V_p$ was therefore obtained from transient analyses for the conduction of heat and the diffusion of mass from the wall, or bulk, to the vapour-liquid interface. This allowed the parameter $V_p$ to be evaluated from

$$V_p = \frac{C_{pL}}{h_{fg}} \sqrt{\frac{K_{th}}{K_m}} \frac{(T_s - T_{sat})}{G} \tag{17}$$

in which $T_s$ is the saturation temperature at the liquid-bubble interface, $K_{th}$ is the thermal diffusivity and $K_m$ is the mass diffusivity. The parameter G was found from

$$G = \frac{(x_w - x_{ws})}{(y_{ws} - x_{ws})} \tag{18}$$

where $x_{ws}$ and $y_{ws}$ are respectively the mass fractions of the most volatile components of liquid and vapour at the liquid-bubble interface. This method is iterative and requires the equilibrium values at the bubble-liquid interface. The method has two regions described by Equations (16a) and (16b). This is because the theoretical approach is only valid when boiling is diffusion controlled, Equation (16b). This occurs when the heat conducted from the wall is used to generate most vapour. This is unlikely when the bulk flow mass fraction of the most volatile component is very low or very high, when Equation (16a) is applicable.

This study was initiated to obtain some understanding of the effects of mass transfer on boiling water-glycerol mixtures at low pressures. Data are available at atmospheric pressure. Existing methods are tested against this

data to investigate their applicability to water-glycerol mixtures. Methods that work at atmospheric pressure are tested against the low pressure data to investigate their extension to low pressures.

## 2. Description of the test facility

The test facility is shown in Figure 1. The liquid level in the rig was set by using the vacuum pump to reduce the pressure in the vessel to about 0.5 bar and allowing liquid to flow into it from the storage tank until the required liquid level was achieved. The vacuum pump was then used to achieve the required test section pressure. Heat was supplied to the evaporator by Joule heating of rod heaters contained within the tubes. Initially, the tube heaters were switched on at 90% of full power. After some time, vapour was generated. This purged any air located in the rig into the hot well before it was expelled to the atmosphere through the vacuum pump. When condensate began to accumulate in the hot well, the liquid entry shut-off valve was opened and the circulating pump was started. The flow rate was set by adjusting the pump control valves until a steady level was obtained in the hot-well sight glass. Liquid from the hot-well was pumped by the circulating pump into the test section via the pre-heater. The inlet temperature can be set by adjustment of the pre-heater. However, this was not used in these tests. Vapour from the vessel was condensed and subcooled before being returned to the hot-well. Steady conditions were achieved in about 3 hours, whence the power controllers were set to produce the required heat flux for the test. Test conditions were achieved in a further 30 minutes.

The test section was manufactured from stainless steel and is shown in Figure 2. It represents a one-quarter scale, thin slice model of an industrial evaporator. The industrial heat exchanger has six coils. These are represented in the model evaporator by the two tube bundles, left and right, offset by 32 mm to replicate the slope of the coils. The main vessel was 1 m high, 0.75 m wide and 98 mm deep. The two smaller vessels were 0.6 m high and were used to vary the pool height from quarter scale up to the level attained in the actual evaporator. The pressure in the test-section vapour space was measured by a Rosemount 3051 absolute pressure transducer, accurate to 0.25% of range. With this uncertainty in the pressure at the free surface, the uncertainty in the corresponding calculated saturation temperature is ±0.9 K. A second, similar pressure transducer measured the pool pressure. This transducer was connected to $p_{pool}$ in Figure 2 and allowed the pool height to be estimated. The tube bundles contained tubes 28.5 mm in diameter in an in-line configuration, with a horizontal tube pitch of 69 mm and a vertical tube pitch of 62.5 mm. The heaters in each coil were regulated by a single power controller. This allowed each coil to operate independently, as is possible on the actual evaporator. A uniform heat flux was

applied to the tubes in this study. The power to each left (three tubes) and right (three tubes) for each coil, top or bottom, was measured by a power meter. The power meter was accurate to ±1% of reading.

Temperatures within the evaporator were measured by k-type thermocouples. The thermocouple locations in the test section are shown in Figure 2. NB: only the right-hand-side of the evaporator contained thermocouples.

The thermocouples were classified into 3 groups. The first group were immersed in the liquid and are referred to as the stream thermocouples. The 'stream' was considered to start at the free surface, flow down the centre line and on to the base of the test section, move across the base and up the side walls, before returning to the free surface. These thermocouples were numbered TS1-TS18 and are shown in Figure 2. The pool height was near TS1 for these tests, giving a pool depth of approximately 2 m, with the top of the tube bundle approximately 1.6 m below the free surface. The thermocouples closest to the shell wall, TS9-TS18 in Figure 2, were 5 mm from the surface. The second group are the tube thermocouples. The tubes were made of brass, had an outside diameter of 28.5 mm, a length of 98 mm and a wall thickness of 5 mm. The tube thermocouples were located within the brass tube walls and were numbered from right to left going top to bottom as TT1-TT18. The third and final group are the fluid thermocouples. These were the thermocouples located in the fluid between the tubes and were also numbered right to left going from top to bottom as TF1-TF11 in Figure 2.

All instruments, except the power meter, were connected to data logging equipment that was linked to a PC and controlled through Labview software. The software allowed monitoring of the instruments during operation and logging of the data when required. The power meter data was entered into a computer file manually. A camera was used to monitor the test section. Each test condition was recorded.

Prior to their installation in the evaporator, all of the thermocouples were calibrated in a water bath. The water bath contained a heater, a stirrer and a resistance thermometer accurate to ±0.1$^{o}$C. The thermocouples, with the necessary compensation cable attached, were connected to the data logging system. The same system was used in the calibrations and in the tests. The uncertainties are summarised in Table 2.

To obtain data set a, each instrument was read once per second over a 2 minute period. Readings were taken a second time, ten minutes later, to obtain data set b. Thereafter, the power controllers were set to produce the next

heat flux and the procedure repeated until the necessary heat-flux range had been achieved. A waiting time of 30 minutes was set between heat flux settlings to allow steady state conditions to be achieved.

## 3. Data processing

The heat-transfer area, *A*, was taken as the outside surface area of a tube. The heat flow, *Q*, to the tubes on the right hand side of a coil, i.e. 3 tubes, was measured by the power meter. The tube heat flux, *q*, was therefore found from

$$q = \frac{Q}{3A} \tag{19}$$

The surface temperature, $T_w$, of each tube wall was found from

$$T_w = T_{tc} - \frac{qD}{2k_B} ln\left(\frac{D}{D-2L_{tc}}\right) \tag{20}$$

where $T_{tc}$ is the measured wall temperature, $D$ is the outside diameter of a tube, $k_B$ is the thermal conductivity of brass, 190 W/mK, and $L_{tc}$ is the depth of the thermocouple from the tube surface, i.e. 2.5 mm. The thermocouple holes were located at better than ±0.5 mm on their pitch circle radius. The uncertainty in the wall temperature therefore varied from ±0.1 K to ±0.2 K as the heat flux increased from 10 to 65 kW/m$^2$. The saturation temperature was evaluated from the local pressure, $p$, found from

$$p = p_s + \rho_L g H \tag{21}$$

where $p_s$ is the measured shell pressure, $\rho_L$ is the density of liquid, $g$ is the gravitational constant and $H$ the depth of the tube centre line from the free surface. The height of the free surface above the pool measurement location was found from

$$H_{pool} = \frac{(p_{pool} - p_s)}{\rho_L g} \tag{22}$$

where $p_{pool}$ was the measured pool pressure. The uncertainties in the pressure at the free surface and in the pool combined to give an uncertainty in the calculated pool height of ±51 mm.

The liquid temperatures associated with each tube were obtained from interpolations using the nearest thermocouples, fluid and stream. Liquid properties were evaluated at the liquid temperature with vapour properties evaluated at the local saturation conditions deduced from the local pressure.

## 4. Experimental results

Two tests series were undertaken at a free surface, absolute pressure of 50 mbar. The first set of tests used water as the working fluid. These had viscosities of typically 0.7 mPas and are referred to as the LV tests. The second set used a glycerol-water mixture with a viscosity of typically 5 mPas. These are referred to as the HV tests. Water data at similar conditions were previously reported in [1]. These data marked as [1] on some figures and are included to show reproducibility.

The fraction of water required in the glycerol-water mixture was estimated to give a viscosity of 5 mPas from the known properties of the mixture. The tests were to be performed at a pressure of 50 mbar, giving a saturation temperature of about 40 $^{o}$C. The desired viscosity was 5 mPas. The required water fraction gave this viscosity at 40$^{o}$C. The glycerol-water mixture was prepared in a graduated, 100 l vessel. The calculated volume of glycerol was put in the vessel before it was filled to the 100 l mark with water. The mixture was subsequently mixed by a powered mixer. The actual water fraction for the test was obtained from viscosity measurements on a sample from the batch. The measurements were obtained over a specified temperature range on a VISCOlab 3000 viscometer. The readings were accurate to ±1%. The mixture water fraction was obtained by altering it in the property routines until a 'best fit' agreement was found between the measured and predicted viscosities. The results are shown in Figure 3, for which the deduced water fraction was 0.38 by mass. The corresponding mole fraction is 0.76.

*4.1 Stream temperatures*

Tests with the tube heat flux set to 65 kW/m$^2$ for the LV and HV test series produced the stream temperatures shown in Figure 4. The values shown are the averages of data sets a and b. Other heat fluxes produced similar results. Included in Figure 4 are the saturation temperatures corresponding to the pressure at the free surface and the evaporator base. The saturation temperature for water varies from 36 $^{o}$C at the free surface to 64 $^{o}$C at the evaporator base. The corresponding values for the glycerol-water mixture are 40 $^{o}$C and 74 $^{o}$C. In both cases the stream temperature is shown to be close to the relevant free surface saturation temperature at the liquid-vapour interface and to rise by a couple of degrees as the pool depth increases. The stream temperature locations, Figure 2, are well distributed throughout the pool. These results are therefore indicative of fluid recirculation taking place, with fluid flashing to the saturation temperature at the free surface before the liquid fraction is returned to the depths of the pool. Thus, this behaviour is not affected by the liquid viscosity.

*4.2 Liquid temperatures*

The liquid temperatures measured in close proximity to the tubes, Figure 2, are shown in Figure 5. They are arranged in terms of tube rows and columns. The tube rows run from bottom to top with the columns running from left to right. Only rows 1 and 6 are shown. The other rows behave similarly. Included in the figure is the local saturation temperature. Both data series have a similar degree of subcooling, with the average row value varying from 25.3 K on row 1 to 23.0 K on row 6 for the LV series and form 26.4 K to 22.3 K for the HV series. All subcoolings are within ±4 K of the averages. Therefore, saturated boiling is not possible as all liquid temperatures are below the saturation temperature.

*4.3 Tube wall temperatures*

The measured tube wall temperatures are shown in Figure 6. Included in the figure are the local saturation temperature and the boiling onset temperature. The boiling onset temperature was taken to occur when the heat flux was related to the wall temperature through, [20],

$$q = \frac{k_L h_{LG} \rho_G (T_w - T_{sat})^2}{8 \sigma T_{sat}} \tag{23}$$

The boiling onset temperature in Figure 6 was found from the applied heat flux so that it represents the maximum temperature that can occur without boiling happening. The saturation and boiling onset temperatures increase with pool pressure (depth). At heat fluxes of 10 and 25 kW/m$^2$, the LV liquid temperatures are below the saturation temperature and are therefore in the single-phase convective heat transfer regime. At heat fluxes of 40, 55 and 65 kW/m$^2$, they are above the boiling onset temperature and are therefore in the subcooled boiling heat transfer regime. The transition between single-phase convection and subcooled boiling therefore occurs within the range of 25-40 kW/m$^2$. At a heat flux of 10 kW/m$^2$, the HV liquid temperatures are below the saturation temperature and are therefore in the single-phase convective heat-transfer regime. At heat fluxes greater than 10 kW/m$^2$, they are above the boiling onset temperature and are therefore in the subcooled boiling heat-transfer regime. The transition between single-phase convection and subcooled boiling therefore occurs within the range of 10-25 kW/m$^2$.

*4.4 Visual observations*

Images of the right hand tube bundle are shown for water and the water-glycerol mixture in Figure 7. Some bubbles are highlighted with a red circle. Very few bubbles are present. This is probably causes by the very high subcoolings present at the tube surfaces. For water, there are no bubbles shown at heat fluxes of 10 and 25 kW/m$^2$, with some shown at heat fluxes of 40, 55 and 65 kW/m$^2$. For the water-glycerol mixture, bubbles are

not present at a heat flux of 10 kW/m$^2$ but are present at all other heat fluxes. It is evident that the water bubbles are much larger than the water-glycerol bubbles. This probably results from the reduced surface tension in the water-glycerol mixture.

## 5. Water-glycerol boiling data

To interpret the low pressure boiling data obtained in this study, information on the mass transfer effects on the boiling behaviour of water-glycerol mixtures is needed. It is extremely difficult to get this information from the test data because only one mass concentration is available. However, data reported in [14] are also available. There are several drawbacks with this data. Water and glycerol only data were not reported, the mixture data were taken at atmospheric pressure and the surface used was stainless steel not brass, as was used in the current tests. Water is a liquid that has been used in multiple boiling experiments. However, boiling data for glycerol have not been found. The low pressure data previously obtained for water, [1], were reasonably well predicted by the Gorenflo correlation [3]. This uses a fluid-specific reference heat-transfer coefficient. The value for water was 5.6 kW/m$^2$K. A value for glycerol is not available. Gorenflo and Kenning, [21], updated the correlation to include a universal standard heat-transfer coefficient and a method to calculate the fluid-specific element. The method derives the heat-transfer coefficient for water from

$$\alpha = \alpha_{ref} F_q F_f F_w F_p \tag{24}$$

where the reference heat-transfer coefficient, $\alpha_{ref}$, is 3.58 kW/m$^2$. The heat flux function, $F_q$, is given by

$$F_q = \left(\frac{q}{q_{ref}}\right)^{ci} \quad \text{with} \quad c_i = 0.9 - 0.3p_r^{0.15} \quad \text{and} \quad p_r = \frac{p}{p_c} \tag{25}$$

where the reference heat flux, $q_{ref}$, is 25 kW/m$^2$. The fluid parameter, $F_f$, is given by

$$F_f = \left(\frac{Lb}{Lb_{ref}}\right)^{0.6} \quad \text{with} \quad Lb = \left[\frac{1}{\sigma}\left(\frac{dp}{dT}\right)\right]_{p_{ref}} \quad \text{and} \quad p_{ref} = 0.1p_c \tag{26}$$

where the reference fluid parameter, $Lb_{ref}$ is 1 (μmK)$^{-1}$. NB: the pressure gradient dP/dT is the saturation line value. The wall parameter, $F_w$, is given by

$$F_w = \left(\frac{Sr}{Sr_{ref}}\right)^{0.133} \left(\frac{\rho}{\rho_{ref}} \frac{k}{k_{ref}} \frac{c}{c_{ref}}\right)^{0.25} \tag{27}$$

where the reference surface roughness, $Sr_{ref}$, is 0.4 μm and the reference wall thermal properties are those for copper. The pressure parameter, $F_p$, is given by

$$F_p = 1.73p_r^{0.27} + \left[6.1 + \frac{0.68p_r}{(1-p_r)}\right] p_r^2 \tag{28}$$

Gorenflo et al [22] have shown that this method significantly underpredicts the value for water. To correct for this, Equation (24) was made to agree with the Gorenflo correlation [3] for a brass surface, consistent with

previous findings, [1]. This was achieved by multiplying the fluid parameter, Lb, by 2.78. Stainless steel values were then obtained by changing the surface thermal parameters, Equation (27). The corrected water heat-transfer coefficients are compared to the values from the Stephan and Abdelsalam water method [19] in Figure 8a. The values were obtained at atmospheric pressure. The agreement is reasonable.

The form of Equation (24) used for fluids other than water is slightly different. The heat flux function is given by

$$F_q = \left(\frac{q}{q_{ref}}\right)^{ci} \qquad \text{with} \qquad c_i = 0.95 - 0.3p_r^{0.3} \qquad \text{and} \qquad p_r = \frac{p}{p_c} \tag{29}$$

and the pressure function by

$$F_p = 0.7p_r^{0.2} + 4p_r + 1.4\frac{p_r}{(1-p_r)} \tag{30}$$

This method was used to determine the glycerol values. These are compared with water-glycerol experimental data obtained at atmospheric pressure for a concentration of 0.33% water in Figure 8b. The agreement suggests that the estimate is reasonable. The water and glycerol value on stainless steel are included in Figure 8a.

The water-glycerol data of Sternling and Tichacek, [14] were presented as tables of heat-transfer coefficient against heat flux for a specified mass fraction of water. Linear interpolations were used to reference these data to a specific heat flux so that values could be compared for a range of water mass fractions at a specified heat flux. Comparison of the data with the correlations of Stephan and Korner [15], Unal [16], Thome and Shakir [17] and Kandlikar [18] are given in Figure 9-12 respectively.

The Kandlikar [18] method requires a diffusion coefficient. Values for water-glycerol mixtures have been presented by D'Errico et al [23]. Wilke and Change, [24], proposed a method for predicting the diffusion coefficient, $D_{wg}$, from the glycerol diffusion coefficient, $D_g$, and the water diffusion coefficient, $D_w$, through

$$D_{wg} = D_g^{X_w} D_w^{(1-X_w)} \tag{31}$$

The glycerol diffusion coefficient is given by

$$D_g = 1.18 \times 10^{-16}\sqrt{M_w}\frac{T_{sat}}{\mu_w \upsilon_g^{0.6}} \tag{32}$$

where $M_w$ is the molecular weight of water and $\nu_g$ is the molar volume of glycerol, given by

$$\upsilon_g = \frac{M_g}{\rho_g} \tag{33}$$

in which $M_g$ is the molecular weight of glycerol. The water diffusion coefficient is given by

$$D_w = 1.18 \times 10^{-16}\sqrt{M_g}\frac{T_{sat}}{\mu_g \upsilon_w^{0.6}} \tag{34}$$

where $\nu_w$ is the molar volume of water, given by

$$\upsilon_w = \frac{M_w}{\rho_w} \tag{35}$$

A comparison of the Wilke and Chang [24] method with the D'Errica et al data, [23], is shown in Figure 13. The agreement is reasonable.

The Stephan and Korner [15] method shows reasonable agreement across the ranges of mass fraction and heat flux, Figure 9. The Unal [16] method also shows good agreement, Figure 10, however, at lower mass fractions and higher heat fluxes, the agreement is not as good. The Thome and Shakir method [17] shows very poor agreement, Figure 11. This is inherent in the method because the boiling range for these data is very large, Equation (9), ensuring a low heat-transfer coefficient prediction that is not evident in the data. The Kandlikar [18] method also shows poor agreement, Figure 12, although its 'shape' is better. This method fails because the sudden reduction at very small glycerol fractions, Equation 16a, does not materialise. The Thome and Shakir [17] and the Kandlikar [18] methods are both methods with a theoretical basis and both approaches significantly under-predict the data. This is because the diffusion processes in them interact with the thermodynamic and transport properties to produce heat-transfer resistances that are much larger than those that actually occur. Thus, for fluids with wide boiling ranges, the mechanisms present during the boiling of binary mixtures are not well understood. For these data at atmospheric pressure, only the empirically based, glycerol specific method of Stephan and Korner [16] or the more universal, but still empirically based, method of Unal [17] show any capability to predict boiling of water-glycerol mixtures.

## 6. Heat-transfer analysis

A precious study, [1], revealed that the tubes operated independent of each other when the pool depth was set to the current levels. For a horizontal cylinder operating in the free convection regime, Churchill and Chu [2] gave the natural convection, heat-transfer coefficient, $\alpha_{nc}$, as

$$\alpha_{nc} = \frac{Nuk_L}{D} = \frac{k_L}{D}\left\{0.6 + \frac{0.387Ra^{\frac{1}{6}}}{\left[1+\left(\frac{0.559}{Pr}\right)^{\frac{9}{16}}\right]^{\frac{8}{27}}}\right\}^2 \tag{36}$$

where $Pr$ is the Prandtl number, given by

$$Pr = \frac{\mu_L c_{pL}}{k_L} \tag{37}$$

in which $\mu_L$ is the liquid viscosity. The Rayleigh number is given by

$$Ra = GrPr = \frac{\rho_L^2 g\beta(T_w - T_L)D^3}{\mu_L^2} Pr \tag{38}$$

in which $T_L$ is the liquid temperature. The thermal expansion coefficient, $\beta$, was obtained from a curve fit to the liquid density across the required temperature range. The fluid properties were evaluated at the film temperature, $T_f$, given by

$$T_f = \frac{(T_w + T_L)}{2} \tag{39}$$

Natural convection took place with increasing heat flux until the onset of nucleate boiling. This occurred when the wall superheat from natural convection balanced with the onset condition, Equation (23), i.e.

$$q_{onb} = \frac{k_L h_{fg} \rho_V (T_w - T_{sat})^2}{8\sigma T_{sat}} = \alpha_{nc}(T_w - T_L) \tag{40}$$

with nucleate boiling continuing thereafter.

For water, the LV data series, the Gorenflo correlation, [20], corrected as described in Section 5, was used for the boiling heat-transfer coefficient, $\alpha_{nb}$. This was of the form

$$\alpha_{nb} = \gamma q_{nb}^n \tag{41}$$

allowing the wall superheat, $\Delta T_{sup}$, to be obtained from

$$\triangle T_{sup} = \frac{q^{(1-n)}}{\gamma} \tag{42}$$

The HV data series were obtained from the water-glycerol binary mixture. For these data, the wall superheat was obtained from Stephan and Korner [16] or the Unal [17] methods as detailed in Sections 1 and 5. For both the LV and HV data series, this method does not allow for partial boiling to develop. The predicted wall super heat was therefore taken as

$$\triangle T_{sup} = minimum\left(\triangle T_{sup,nc}, \triangle T_{sup,nb}\right) \tag{43}$$

Equation (40) gave boiling onset wall superheats of typically 5 K for the LV data series. This translates to an onset heat flux of 34 kW/m$^2$. This requires the data taken at heat fluxes of 10 and 25 kW/m$^2$ to be in the natural convection regime and those obtained at heat fluxes of 40, 55 and 65 kW/m$^2$ to be in the subcooled nucleate boiling regime. This is consistent with the visual observations, Figure 7. Equation (40) gave boiling onset wall

superheats of typically 4 K for the HV data series. This translates to an onset wall heat flux of 13 kW/m$^2$. This requires the data taken at a heat flux of 10 kW/m$^2$ to be in the natural convection regime with all others being in the subcooled boiling regime. This is also consistent with observations, Figure 7.

The accuracy of the wall superheat predictions was estimated from a statistical analysis of the predicted and measured wall temperature differences. These were defined as the difference between the wall and liquid temperatures.

A comparison between the measured and predicted wall temperature differences for the LV data series using the Churchill and Chu correlation, [2], for the natural convection regime and the corrected Gorenflo correlation, [20], for the subcooled nucleate boiling regime shows little difference in the behaviour of the columns. This combined approach over-predicts the data with an average difference of -6.3%, -6.8% and -2.4% for columns 1, 2 and 3 respectively. The corresponding rms differences are 7.9%, 8.6% and 7.1%. Overall, the average and rms differences are -5.2% and 7.9% respectively. These predictions confirm the findings from [1] that the Gorenflo correlation, [3], adequately predicts boiling heat-transfer of water at low pressures and that the latest method, [20] significantly under-predicts them, unless it is corrected, as it is herein.

For the HV data series, predictions were made by using the Churchill and Chu correlation, [2], for natural convection and the Gorenflo correlation, [20], for nucleate boiling, corrected for water and as is for glycerol. The Stephan and Korner correlation, [16], was used to account for mixture effects. The method predicts the data with an average difference of 6.1%, 8.6% and 11.5% for columns 1, 2 and 3 respectively. The corresponding rms differences are 17.8%, 19.8% and 20.2%. Overall, the average and rms differences are 8.8% and 19.3% respectively. Taking a similar approach with the Unal correlation, [17], used to account for mixture effects predicts the data with an average difference of -2.9%, -0.6% and 2.1% for columns 1, 2 and 3 respectively. The corresponding rms differences are 10.7%, 11.0% and 10.2%. Overall, the average and rms differences are -0.5% and 10.7% respectively. Thus, the predictions from this approach are reasonably centred on the data. The Stephan and Kroner method, [16], under-predicts the data and does so less accurately than the Unal method [17].

A comparison between the measured and predicted wall superheats for the Unal-based approach is shown in Figure 14. Data sets a and b, taken at the same conditions ten minutes apart, are both shown. Figure 14 shows reasonable agreement between the Churchill and Chu correlation, [2], at a heat flux of 10 kW/m$^2$. The data behaviour at higher heat fluxes are consistent with pool boiling, in that the wall superheat increases with increasing heat flux. The upper and lower limits shown in Figure 14d are set at ±30%, with the data for columns

1, 2 and 3 shown in black, red and blue respectively. There is little difference between the behaviour of the columns. The data obtained at a heat fluxes of 25 and 40 kW/m$^2$ are reasonably well predicted by the Gorenflo-Unal approach. However, further increases in heat flux produce larger increases in the measured wall superheats than those predicted. Overall though, the approach is reasonable. The statistics of the comparisons are summarised in Table 1.

## 7. Discussion and conclusion

Water and glycerol-water mixture, heat-transfer data have been obtained at a pressure of 50 mbar for a range of heat fluxes. For both fluids, the liquid temperatures in the pool were found to be reasonably uniform and controlled by the pressure at the free surface, Figure 4. This led to subcoolings of up to 31 K at the tube surfaces for both fluids, Figure 5. The reasonably uniform pool temperatures suggest that the liquids re-circulate within it and that only subcooled nucleate boiling is possible at appropriate heat fluxes.

The data indicate that boiling occurs in the mixture at a lower heat flux than in water, 10-25 kW/m$^2$ compared to 25-40 kW/m$^2$. However, the boiling onset wall superheats are similar, 5 K for water and 4 K for the mixture. The boiling onset heat fluxes are shown to be reasonably accurately predicted by Equation (40), 34 kW/m$^2$ for water and 13 kW/m$^2$ for the mixture. Thus, the natural convection, heat-transfer coefficient for the mixture is smaller than that for water, i.e. the lower boiling onset heat flux results from fluid property changes that reduce the natural convection coefficient from 1150 W/m$^2$K for water to 440 W/m$^2$K for the glycerol-water mixture.

Water-glycerol data at atmospheric pressure, [14], are shown to be reasonably well predicted by the pure fluid correlation of Gorenflo and Kenning, [21], when the water value is corrected, as described in section 5, and the glycerol values are as is. The correction methods of Stephan and Korner [16] and Unal [17] are reasonable for water-glycerol mixtures at atmospheric pressure whereas those of Thome and Shakir [18] and Kandlikar [19] are not, Figure 9-12. This is evidence of the poor understanding that currently exists of the mechanisms present in boiling binary mixtures with a wide boiling range. The low water concentration data values of [14] are compared with the correction methods of Stephan and Korner [16] and Unal [17] in Figure 8b to further verify the approach taken for pure glycerol.

Heat is transferred to the water and the glycerol-water mixture by natural convection at heat fluxes of 10-25 kW/m$^2$ and 10 kW/m$^2$ respectively. The wall temperature of both fluids is predicted reasonably well by the Churchill and Chu correlation [2], Figure 13, Table 1.

At atmospheric pressure, the Stephan and Korner [16] method is more reliable than Unal [17]. This is not the case at low pressure, where the situation is reversed. This suggests that the pressure correction element, Equation (2), does not extend the method to low pressures.

At low pressure, heat is transferred to the water by subcooled boiling at heat fluxes greater than 25kW/m$^2$ and the water data are reasonably well described by Gorenflo [3]. At low pressure, heat is transferred to the glycerol-water mixture by subcooled boiling at heat fluxes greater than 10 kW/m$^2$. These mixture data are reasonably well described when the pure fluid method of Gorenflo et al [21], when corrected for water as described in Section 5 and as is for glycerol, are coupled to the mixture correction method of Unal, [17], Figure 14, Table 1. However, the Unal method, [17], becomes less effective at larger heat fluxes. Further work on the mixture effect will be required.

The wall temperature for the glycerol-mixture is much greater than that for water, Figure 6. However, the measured temperatures are reasonably well predicted by the heat-transfer correlations [3, 17, 21], Table 1. Thus, the higher wall temperatures are brought about by the poorer heat-transfer characteristics of the glycerol-water mixture. These changes are induced by the change in the fluid properties and, during boiling, the added heat-transfer resistance due to the effects of mass-transfer at the liquid-vapour interface.

**Acknowledgement**

Heriot-Watt University gratefully acknowledges the funding provided for this work by Sellafield Sites Ltd. and the National Nuclear Laboratory.

**References**

1. McNeil D.A., Burnside B.M., Rylatt D.I., Elsaye E.A. and Baker S, Shell-side boiling of water at sub-atmospheric pressure, Int J Heat and Mass Transfer, Vol 85, pp 488-504, 2015.
2. Churchill S.W. and Chu H.H.S., 1975, Correlating equations for laminar and turbulent free convection from a vertical plate, Int. J. Heat Mass Transfer, Vol. 18, pp. 1323-1329.
3. Gorenflo D., 1993, Pool boiling, VDI-Heat Atlas, VDI-Verlag, Dusseldorf.
4. Feldmann, H. and Luke A, 2008, Nucleate boiling in water for different pressures, Int Refrigeration and Air Conditioning Conference, Purdue, July 14-17.
5. Minchenko, F.P. and Firsova, E.V., 1969, Heat transfer to water and water-lithium salt solutions in nucleate pool boiling. Problems of heat transfer and hydraulics of two-phase media, S.S. Kutateladze ed Pergamon Press, Oxford, pp. 137-151.

6. Gordova, A.K., Kabankov, O.N., Yu K., Martinov V.V. and Yagov, 1979, Effet of the material and of the thickness of the heating surface on the heat transfer rate in boiling of water and ethanol at subatmospheric pressures, Heat Transfer Soviet Research, 11, Vol. 3, pp.44-52.
7. M. G. Cooper, 1984, Heat flow rates in saturated nucleate pool boiling – A wide ranging examination using reduced properties, Advances in Heat Transfer, Academic press, Orlando, Vol. 16, pp 157-239.
8. I A Raben, R T Beaubouef and G E Commerford, 1965, A study of heat transfer in nucleate pool boiling of water at low pressure, Chemical engineering progress series, AIChE New York 1951-1971, pp 249-257.
9. F Giraud, R Rulliere, C Toublanc, M Clausse and J Bonjour, 2013,Experimental study of water pool boiling at very low pressure on a vertical or horizontal surface, 4th IIR conference on thermophysical properties and transfer processes of refrigeration, Delft, The Netherlands, Paper TP-035.
10. F Giraud, R Rulliere, C Toublanc, M Clausse and J Bonjour, 2015, Experimental evidence of a new regime for boiling of water at subatmospheric pressure, Experimental thermal and fluid science, Vol. 60, pp 45-53.
11. L Yu, S Xu, G Ma and J Wang, 2015, Experimental research on water boiling heat transfer on horizontal copper rod surface at sub-atmospheric pressure, Energies, Vol 8, pp 10141-10152.
12. B Zajaczkowski, T Halon and Z Krolicki, 2016, Experimental verification of heat transfer coefficient for nucleate boiling at sub-atmospheric pressure and small heat fluxes, Heat and Mass transfer, Vol 52, pp 205-2015.
13. G P Celata, M Cumo and T Setaro, 1994, A review of pool and forced convective boiling of binary mixturtes', Experimental thermal and fluid science, Vol 9, pp 367-381.
14. C V Sternling and L J Tichacek, 1961, Heat transfer coefficients for boiling mixtures, Chen Eng Science, Vol. 16, pp297-337.
15. Stephan, K. and Korner, M., Calculation of heat transfer in evaporating binary mixtures, Chem-Ing Tech, Vol 41, pp409-417, 1969.
16. Unal, H.C., Prediction of nucleate pool boiling heat transfer coefficients for binary mixtures, Int. J. Heat Mass Transfer, Vol. 29, pp. 637-640, 1986.
17. J R Thome and S Shakir, A new correlation for nucleate pool boiling of aqueous mixtures, 1987, AIChE symposium series, Issue 257, pp 46-51.
18. S G Kandlikar, 1998, Boiling heat transfer with binary mixtures: Part 1 – A theoretical model for pool boiling, Vol 120, pp380-387.
19. K Stephan and M Abdelsalam, 1980, Heat transfer correlations for natural convectionboiling, Int J Heat and Mass Transfer, Vol. 23, pp73-87.
20. Sato T. and Matsumurs H., 1963, On the condition of incipient subcooled boiling and forced convection, Bull JSME, pp392-398.
21. D Gorenflo and D B R Kenning, 2010, Pool boiling, Chapter H2, VDI-Heat Atlas, second edition, Springer Berlin.
22. Gorenflo, D., Baumhogger, E., Herres, G. and Kotthoff, S., Prediction methods for pool boiling heat transfer: A state-of-the-art review, Int J of Refrigeration, Vol 43, pp 203-226, 2014.
23. G D'Errico, O Ortona, F Capuano and V Vitagliano, 2004, Diffusion coefficients for the binary system glycerol + water at 25 $^{o}$C. A velocity correlation study, J Chem Eng Data, Vol 49, pp1665-1670.
24. C R Wilke and P Chang, 1955, Correlation of diffusion coefficient in dilute solutions, AIChE J, Vol 1, pp 264-270.

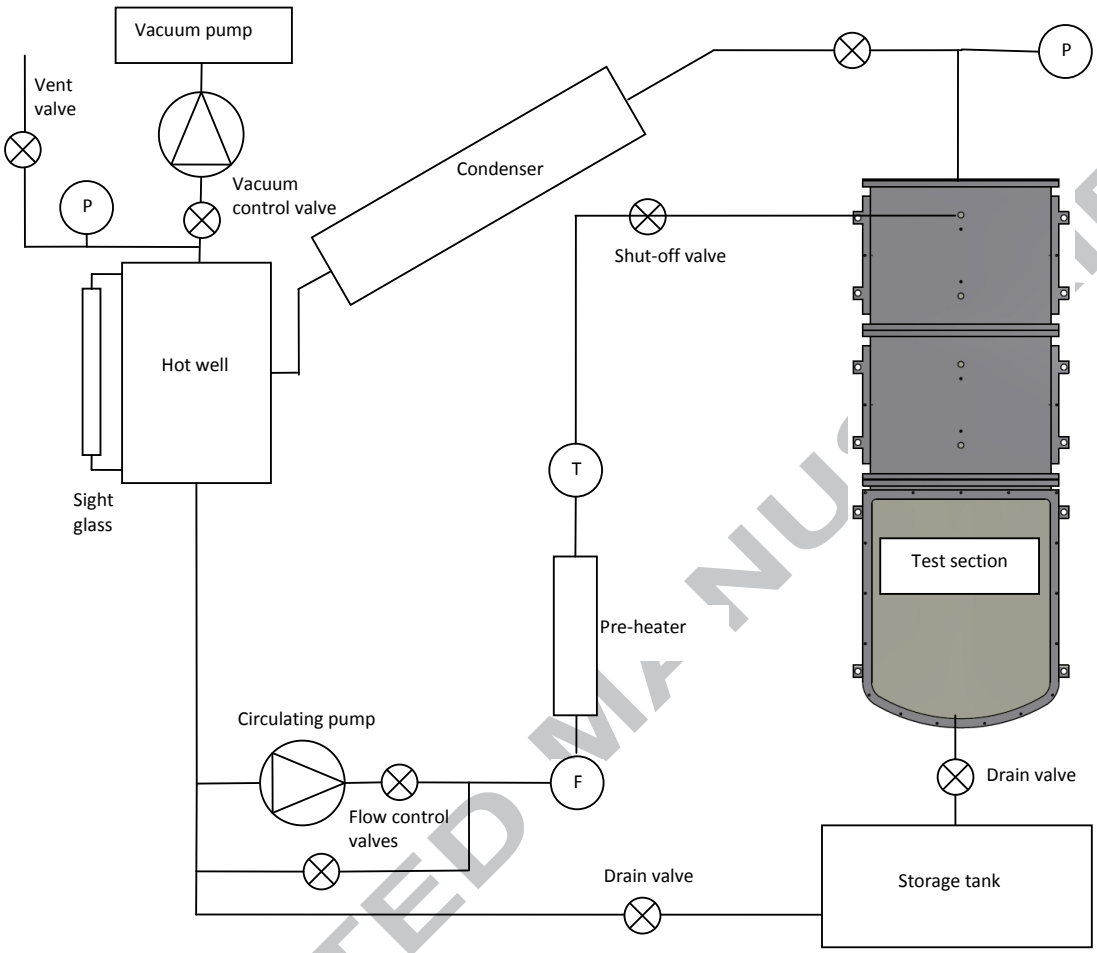


Figure 1: Plant layout

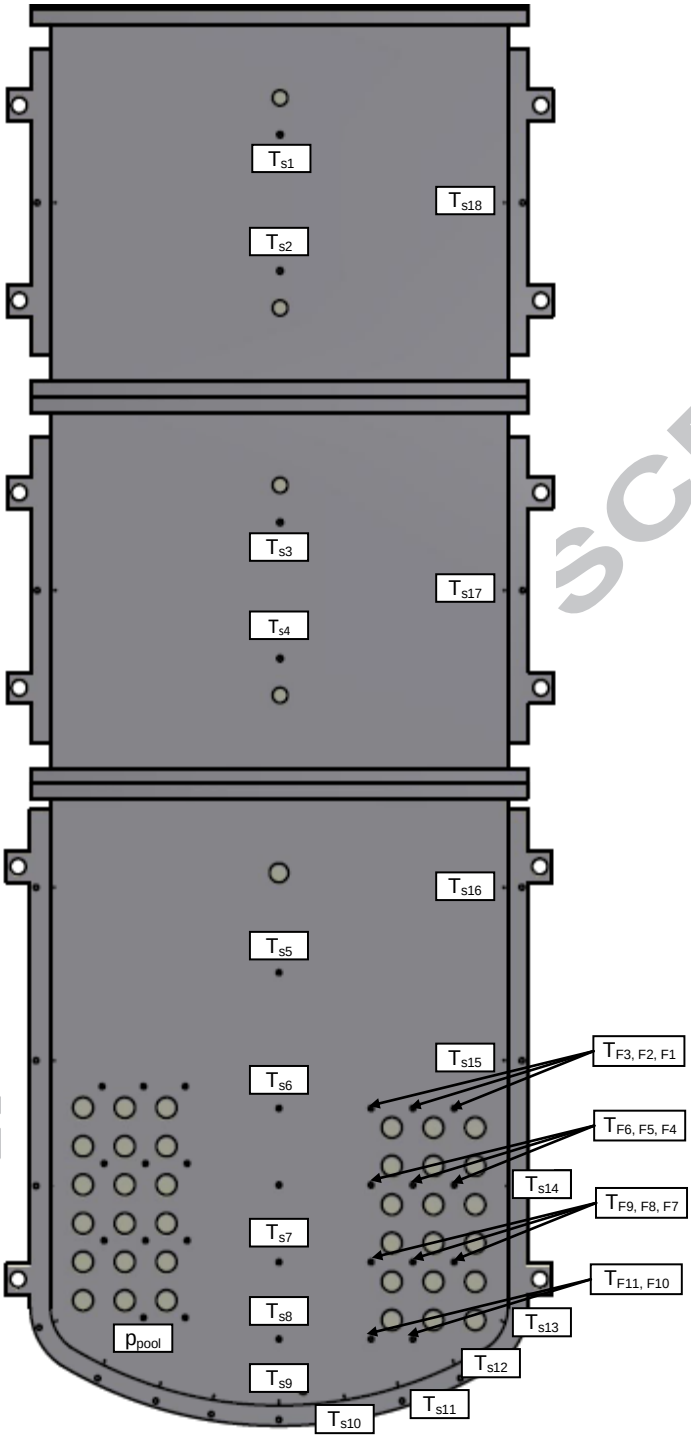


Figure 2: Thermocouple locations

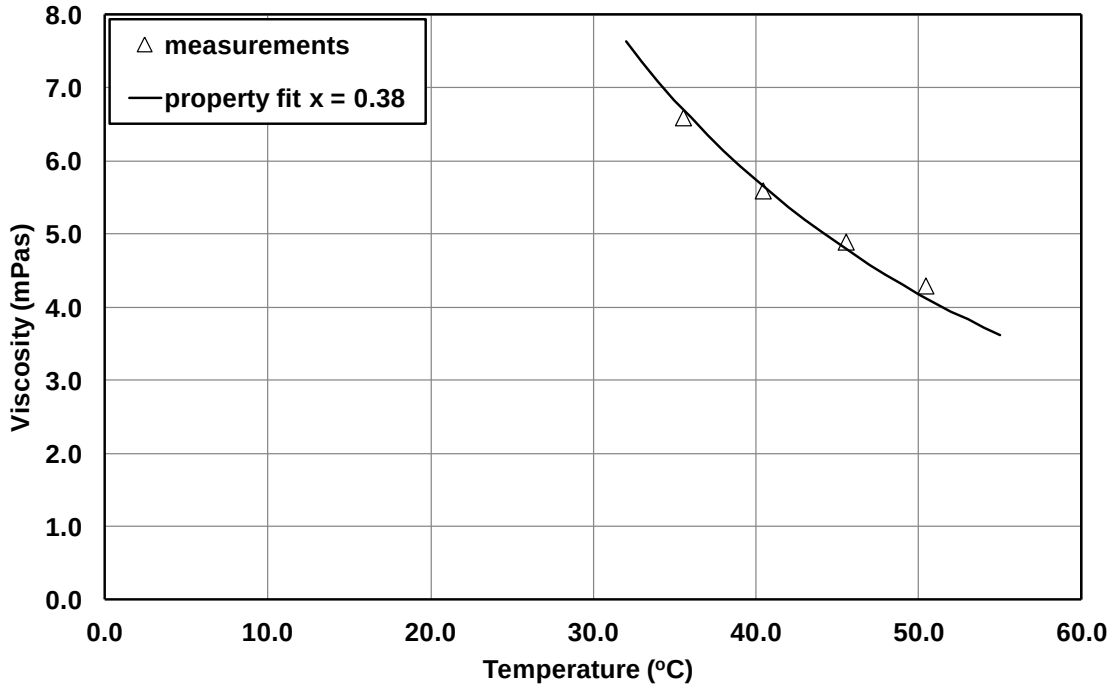


**Figure 3: Variation of viscosity with temperature**

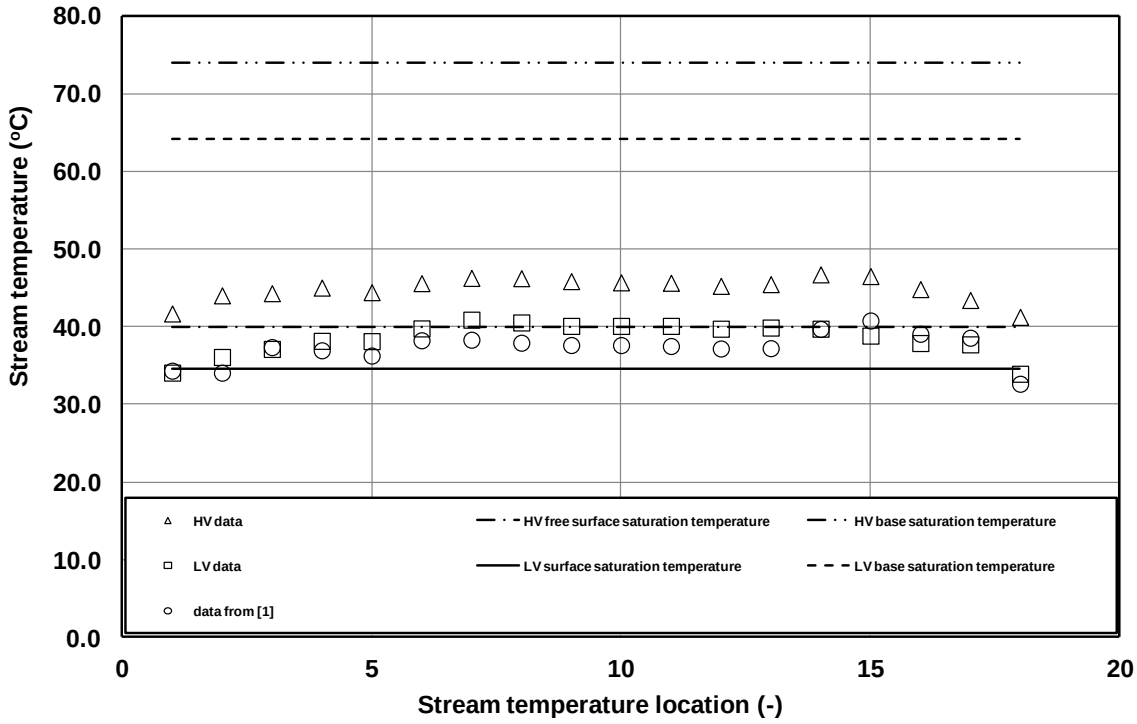


**Figure 4: Variation of stream temperature with rig location**

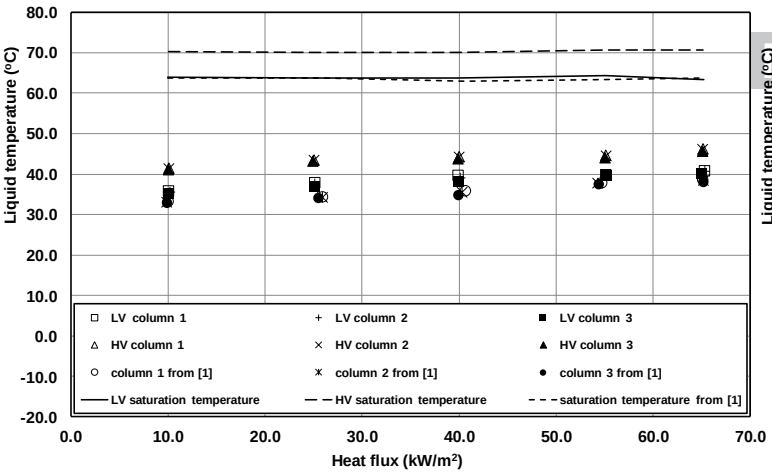


Figure 5a: Variation of liquid temperature with heat flux on Row 1

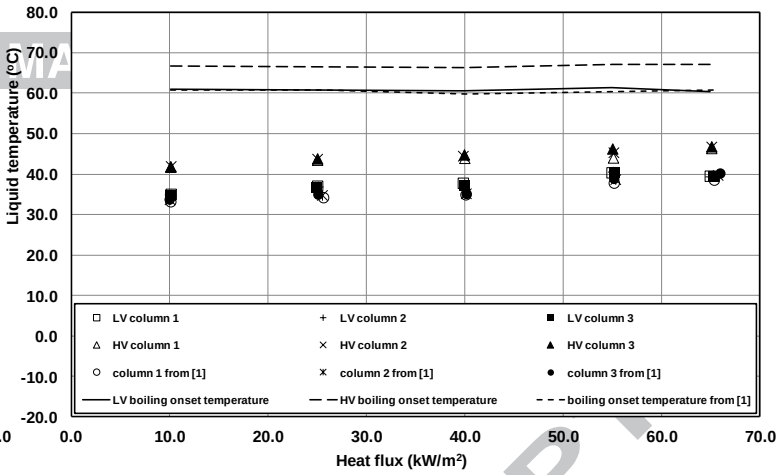


Figure 5b: Variation of liquid temperature with heat flux on Row 6

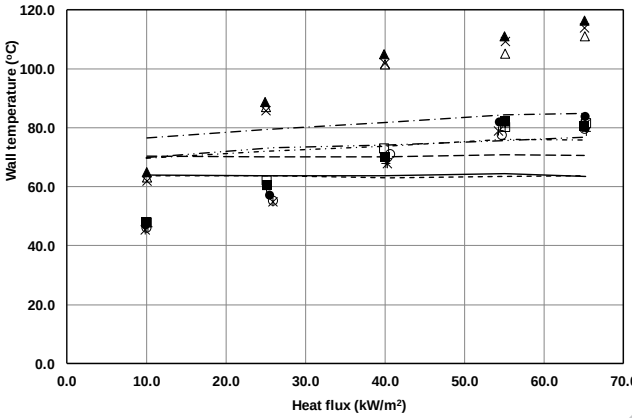


Figure 6a: Row 1

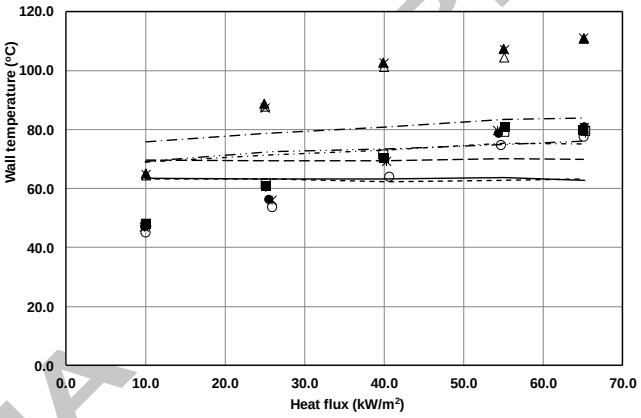


Figure 6b: Row 2

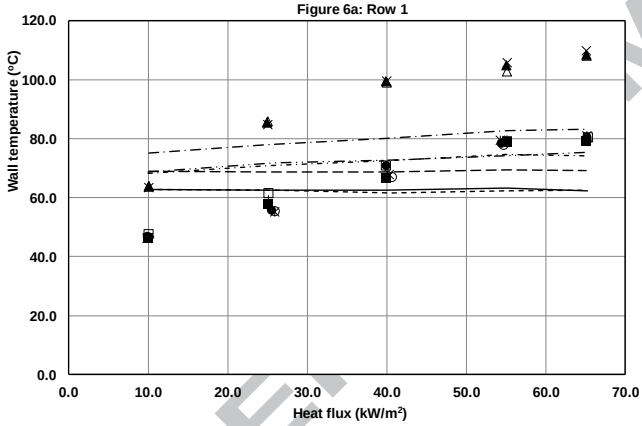


Figure 6c: Row 3

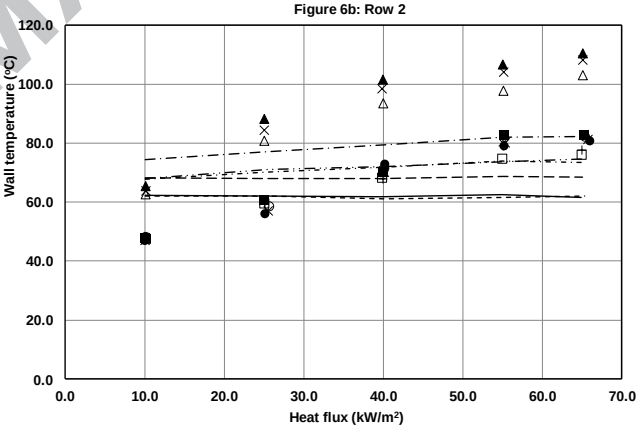


Figure 6d: Row 4

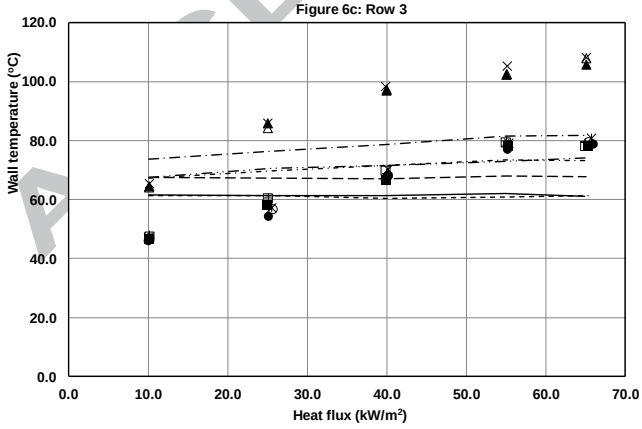


Figure 6e: Row 5

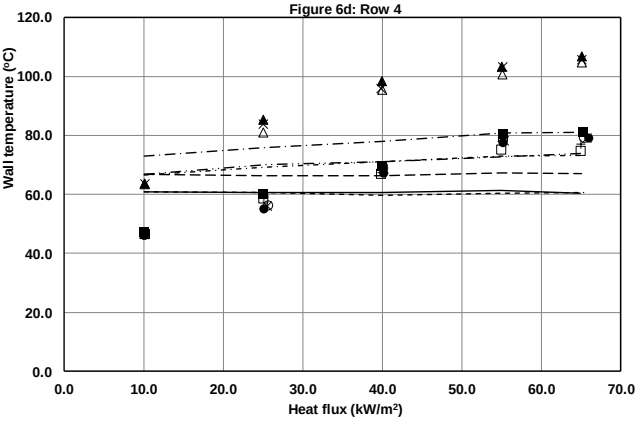


Figure 6f: Row 6

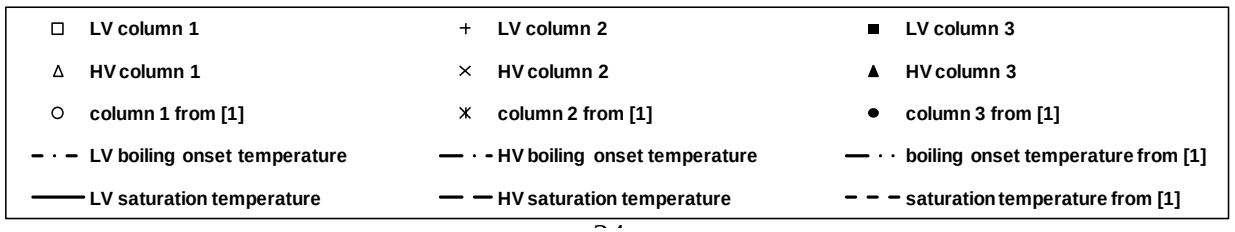


**Figure 6: Wall temperature variation with heat flux**

**Water**

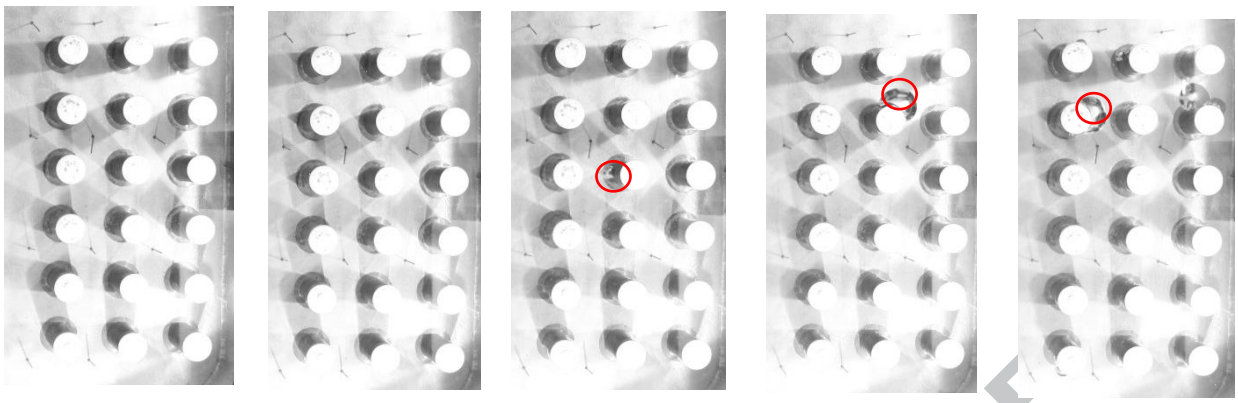

**Water-glycerol mixtures**

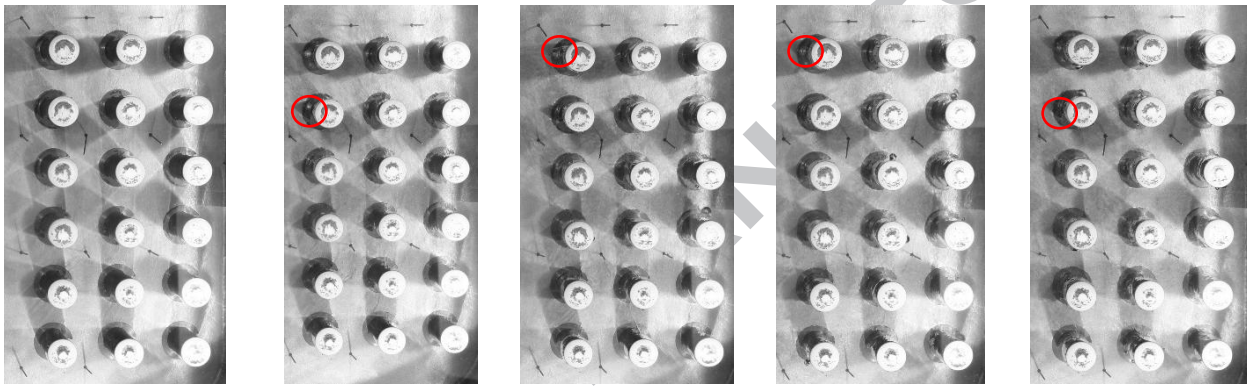

$q = 10\ kW/m^2$ $q = 25\ kW/m^2$ $q = 40\ kW/m^2$ $q = 55\ kW/m^2$ $q = 65\ W/m^2$

**Figure 7: Tube bundle images of water and water-glycerol mixtures**

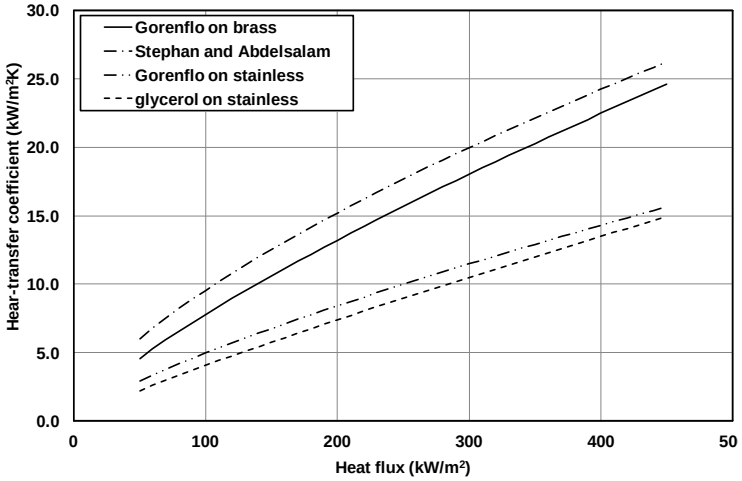


**Figure 8a: Boiling water heat-tranfer coefficients**

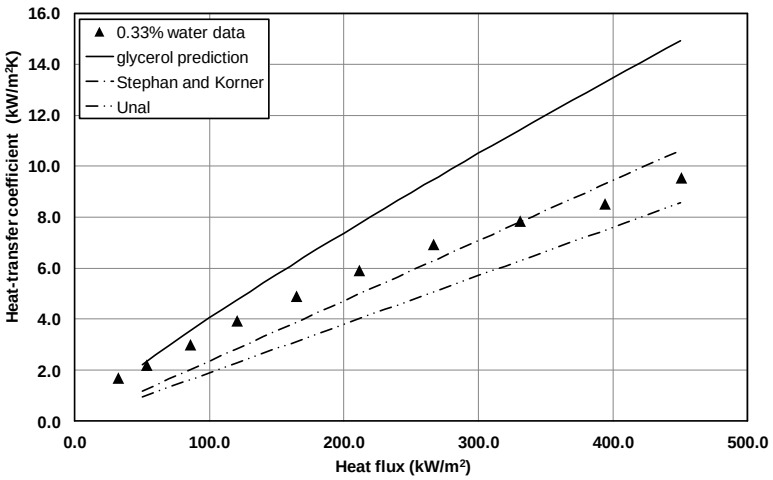


**Figure 8b: Variation of heat-transfer coefficient with heat flux**

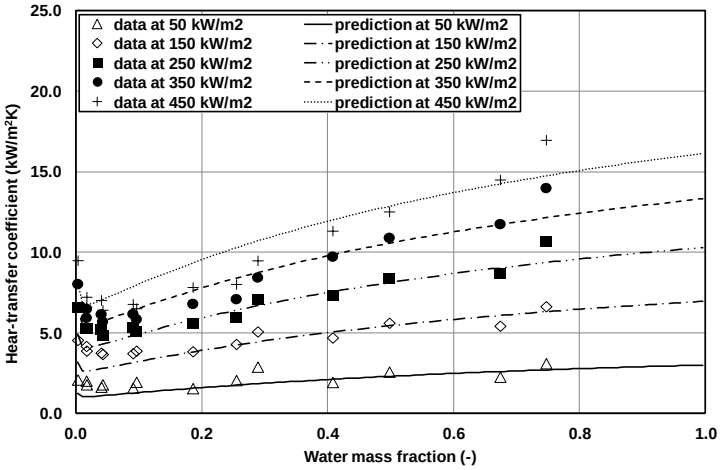


Figure 9: Comparison of data with the method of Stephan and Korner

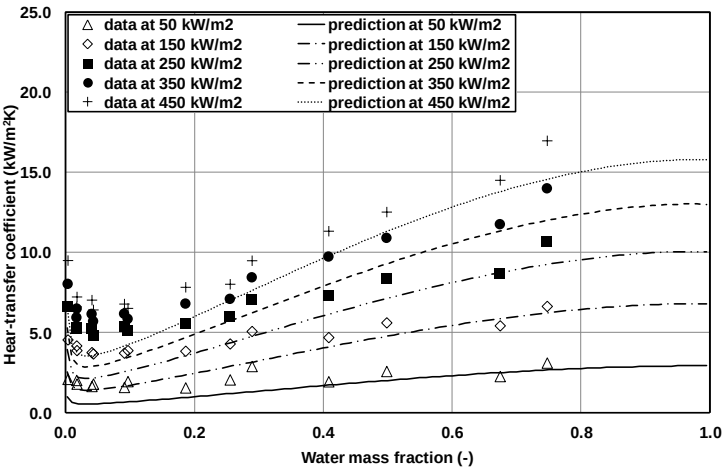


Figure 10: Comparison of data with the method of Unal

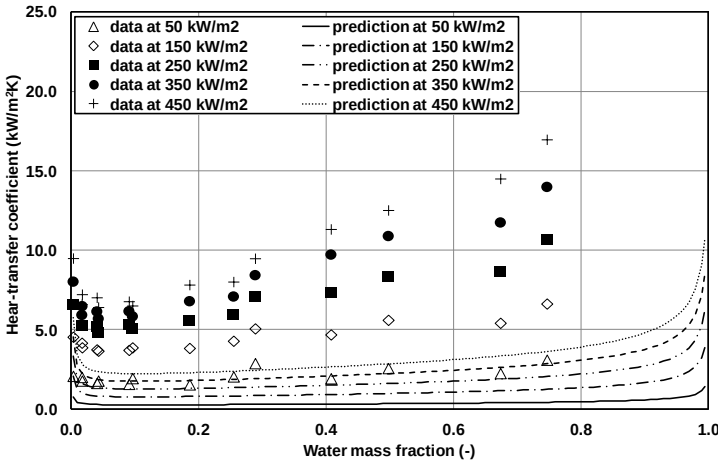


Figure 11: Comparison of data with the method of Thome and Shakir

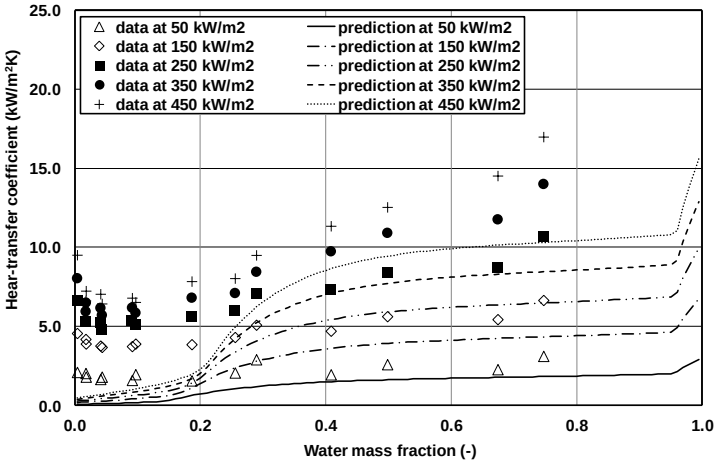


Figure 12: Comparison of data with the method of Kandlikar

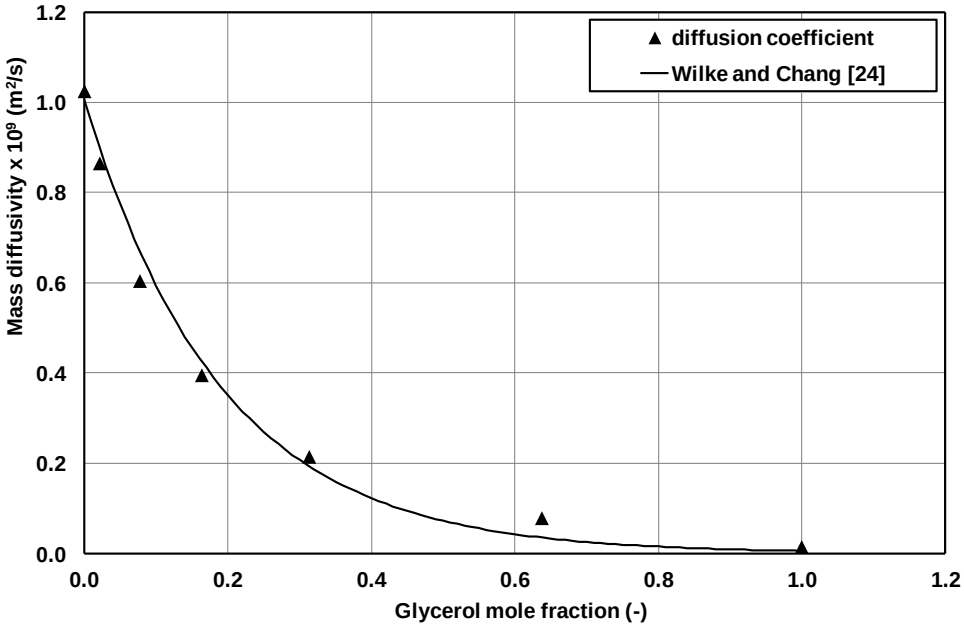


Figure 13: Variation of mass diffusivity with glycerol concentration

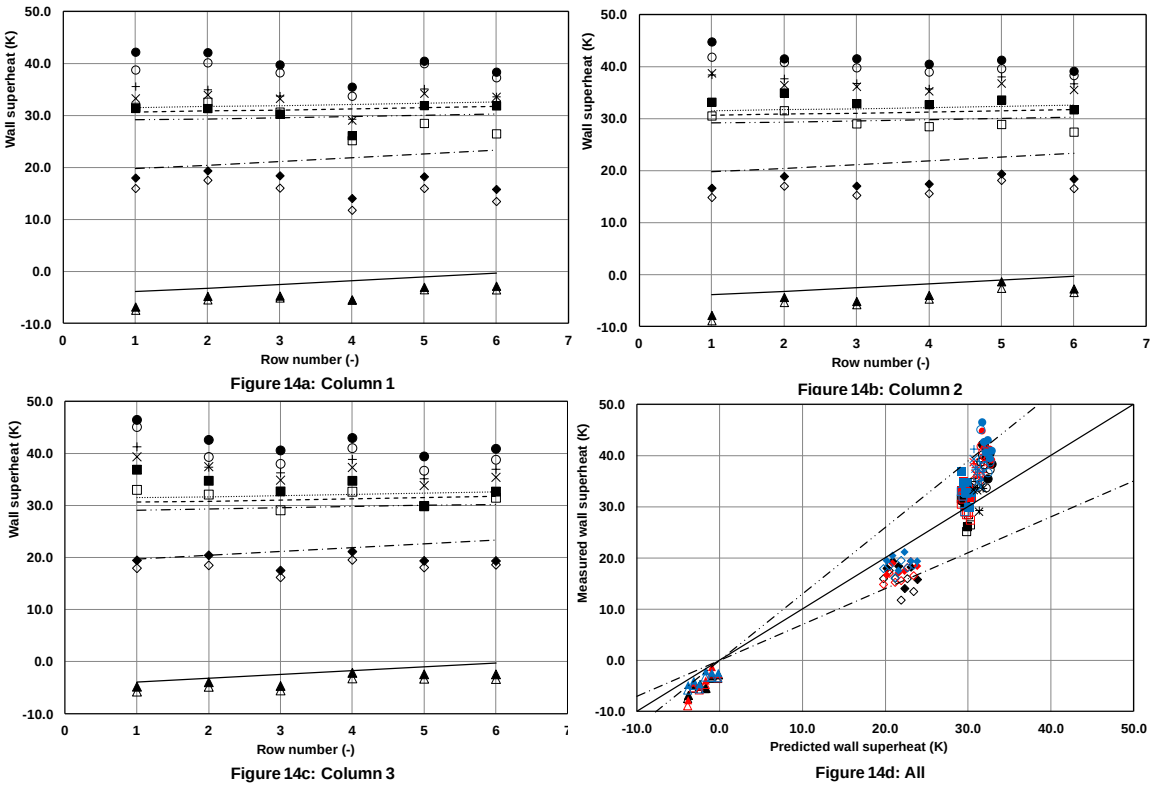


**Figure 14: Wall superheat comparisons between the Unal-base method and the HV data set**

| | | Column 1 | | Column 2 | | Column 3 | | All | |
|---|---|---|---|---|---|---|---|---|---|
| Test series (-) | Mixture method (-) | Average error (%) | RMS error (%) | Average error (%) | RMS error (%) | Average error (%) | RMS error (%) | Average error (%) | RMS error (%) |
| LV | none | -6.3 | 7.9 | -6.8 | 8.6 | -2.4 | 7.1 | -5.2 | 7.9 |
| HV | Stephan and Korner | 6.1 | 17.8 | 8.6 | 19.8 | 11.5 | 20.2 | 8.8 | 19.3 |
| HV | Unal | -2.9 | 10.7 | -0.6 | 11.0 | 2.1 | 10.2 | -0.5 | 10.7 |

Table 1: Summary of methods statistics

| Item | uncertainty |
|---|---|
| pool height | ± 51 mm |
| power | ± 1 % |
| pressure (absolute) | ± 0.25 % of range |
| saturation temperature | ± 0.9 K |
| temperatures (measured) | ± 0.1 K |
| temperatures (wall) | ± 0.2 K |
| viscosity | ± 1 % |

Table 2: Summary of uncertainties

| | | Column 1 | | Column 2 | | Column 3 | | All | |
|---|---|---|---|---|---|---|---|---|---|
| **Test series (-)** | **Mixture method (-)** | **Average error (%)** | **RMS error (%)** | **Average error (%)** | **RMS error (%)** | **Average error (%)** | **RMS error (%)** | **Average error (%)** | **RMS error (%)** |
| LV | none | -6.3 | 7.9 | -6.8 | 8.6 | -2.4 | 7.1 | -5.2 | 7.9 |
| HV | Stephan and Korner | 6.1 | 17.8 | 8.6 | 19.8 | 11.5 | 20.2 | 8.8 | 19.3 |
| HV | Unal | -2.9 | 10.7 | -0.6 | 11.0 | 2.1 | 10.2 | -0.5 | 10.7 |

Table 1: Summary of methods statistics

| **Item** | **uncertainty** |
|---|---|
| pool height | ± 51 mm |
| power | ± 1 % |
| pressure (absolute) | ± 0.25 % of range |
| saturation temperature | ± 0.9 K |
| temperatures (measured) | ± 0.1 K |
| temperatures (wall) | ± 0.2 K |
| Viscosity | ± 1 % |

Table 2: Summary of uncertainties